

## MASTERING THE DEFECTIVITY: PREREQUISITE FOR HIGH EFFICIENCY SILICON HETEROJUNCTION SOLAR CELLS

Renaud Varache<sup>a,\*</sup>, Jérémy Dahan<sup>a,b</sup>, Julien Hotel<sup>a</sup>, Wilfried Favre<sup>a</sup>, Adrien Danel<sup>a</sup>, Charles Roux<sup>a</sup>

<sup>a</sup>Univ Grenoble Alpes, CEA, LITEN, DTS, LHET, INES, F-73370, Le Bourget-du-Lac, France

<sup>b</sup>Independent research consultant, 5 rue Mathurin Regnier 75015 Paris Paris, France

\*Corresponding Author: Renaud Varache (renaud.varache@cea.fr) +33 479 792 873

**ABSTRACT:** The crystalline (*c*-Si) wafer passivation quality is known to be a key factor in the performance of high efficiency silicon based solar cells, among them silicon heterojunction cells (SHJ). During the cell fabrication process, wafers are manipulated via different handling systems entering in contact with the bare or weakly protected *c*-Si surface. Here the passivation quality brought by amorphous silicon (*a*-Si:H) is likely to be locally degraded. The amount of defectivity is revealed by spatially resolved photoluminescence. In this contribution, an image processing software HETLUMTOOL developed internally at CEA is introduced. It allows for the quantification of the defectivity, that can then be linked to cell performance. The cell power conversion efficiency loss due to the defectivity amounts roughly 1.5% for cells produced at CEA [2018 data]. HETLUMTOOL features several options useful in a production line as a check of the correct behavior of the wafer transport system, for various cell technologies. Works done at CEA to reduce the defectivity took an important part in the achievement of the 24.63% cell (total area - 244.3 cm<sup>2</sup>) certified SHJ cell produced on an industrial set of tools. More recently a power conversion efficiency of 25.00% was reached (212.84cm<sup>2</sup>).

Keywords: Heterojunction, Defects, Photoluminescence

### 1 INTRODUCTION

The availability of high carrier lifetime crystalline silicon (*c*-Si) wafers and their excellent surface passivation by hydrogenated amorphous silicon (*a*-Si:H) has led silicon heterojunction solar cells (SHJ) to the forefront of high efficiency silicon based solar cells [1], [2]. In their way to approach their maximum theoretical power conversion efficiency, SHJ cells are hindered by several practical obstacles, among them the defectivity – i.e. the local lack of surface passivation due to contaminants or scratches originated by the environment or the handling systems [3], [4], [5]. As production line throughputs are due to increase for higher competitiveness, the defectivity issue is expected to become more and more critical and is worth a particular focus for R&D purposes (improvement of cell efficiency) as well as in an industrial framework (production line operability).

We report here on the characterization of SHJ cells production lots via photoluminescence (PL). An in-house developed image processing software HETLUMTOOL then allows for a quantification of the defectivity.

After exposing details on the cell fabrication, characterization setup and image processing tool, correlation results between defectivity and cell performance are derived. Several features developed within HETLUMTOOL are introduced and their ability to support the operation of a production line is shortly discussed.

### 2 EXPERIMENTAL & SOFTWARE

#### 2.1 Cell fabrication & properties

Solar cells under investigation here are rear emitter, silicon heterojunction cells fabricated on an industrial set of equipment at the CEA semi-industrial pilot line. As a standard, the 156x156 mm<sup>2</sup> high quality n-type crystalline silicon wafers (typically multi-millisecond bulk carrier lifetime, resistivity around 1 ohm cm) are passivated with intrinsic amorphous silicon (*a*-Si:H),

covered with the doped *a*-Si:H layers (n on front side, p on back side). The Indium Conductive Oxide (ITO) deposited on both sides allows the charge carriers to be conducted up to the silver-paste screen printed metallization grid.

#### 2.2 Photoluminescence & image processing

Photoluminescence images of finished cells are acquired via the BT Imaging PL setup. These images are then processed with the in-house developed software HETLUMTOOL. As illustrated in Figure 1, the raw image *I* is first finely rotated to facilitate the subsequent steps. Then the edges of the cell are precisely located and the cell isolated from the background. In order to make it possible to compare cell technologies with different metallization schemes, the fingers and busbars are removed, via DFT techniques and inpainting respectively. The image being now “cleaned” of any unwanted features, a low frequency, background image *B* is extracted.

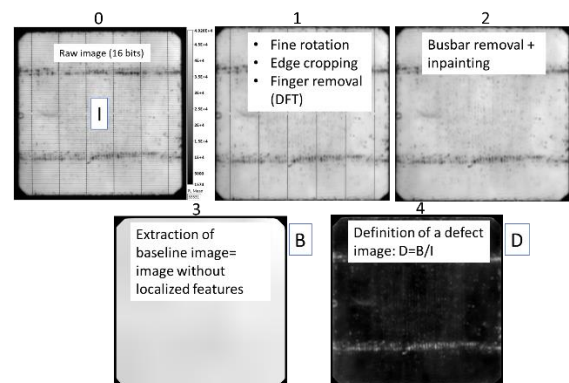


Figure 1: Image processing sequence within HETLUMTOOL

The defect image is eventually defined as  $D=B/I$ : only the local loss of PL signal remains on *D*.

As the implied open-circuit voltage  $iV_{oc} \propto \ln(\alpha I_{PL})$  [6] where  $\alpha$  is a constant and  $I_{PL}$  is the PL signal,  $D_{xy}$  can be seen as a local drop of voltage:  $\Delta V_{xy} \propto \ln(D_{xy})$ ,  $x$

and y scanning the pixels within the cell. Therefore the metric used to quantify the defectivity is defined as:

$$M_D = \ln \left[ \frac{1}{N_{mask}} \sum_{x,y \in mask} D_{xy} \right]$$

$N_{mask}$  being the number of pixel composing the cell image, and “mask” designating the cell area.

$M_D$  will be used in the following as a quantification of the global defectivity for a given cell.

HETLUMTOOL offers several features including ::

- Computation of dedicated metrics for specific types of defects like “varicella” (punctual, randomly distributed defects), belts marks (longitudinal marks across the cell), defects close to the edge, cracks, etc.
- Ability to process non metallized cells, busbarless cells and cells with busbars (unrestricted number)
- Compatibility with half-cells and full cells of any size (M2, M6, M12...)
- Single cell and batch image processing
- Correlation with IV performances + fit
- Storage of previous results in database for later comparison

This makes HETLUMTOOL, together with PL, a powerful characterization tool for both R&D and industrial purposes.

### 3 EFFICIENCY LOSS DUE TO DEFECTIVITY

The main objective in developing HETLUMTOOL was to be able to quantify how much of cell efficiency is lost due to the defectivity. To do so, around 400 cells produced on the pilot line, were measured in PL and the images treated in HETLUMTOOL.

The open circuit voltage  $V_{oc}$ , the short circuit-current  $I_{sc}$ , the fill factor  $FF$  and the power conversion efficiency  $\eta$  are plotted as a function of the global defectivity metric  $M_D$  (Figure 2).

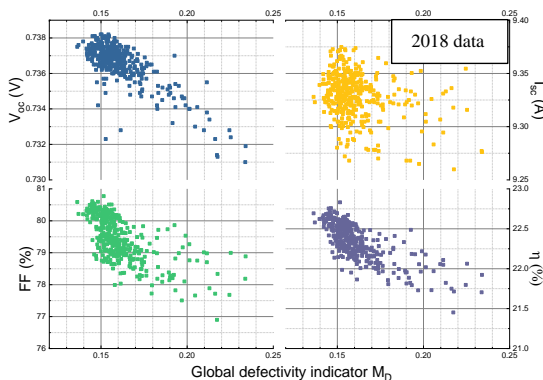


Figure 2: IV parameters of cells produced at CEA, plotted as a function of the global defectivity metric  $M_D$ .

$I_{sc}$  shows no dependence on  $M_D$ , whereas a clear loss in  $V_{oc}$  and  $FF$  is associated with  $M_D$ . Most of the resulting drop in  $\eta$  is actually driven by the up to 3% drop in  $FF$ . The detailed dependence of cell parameters on  $M_D$  and the underlying physics is documented in the recent paper from Giglia et al [5].

A linear fit of Figure 2 leads to the coarse description of the  $\eta$  dependence on  $M_D$ :  $\eta = 24.06 - 10.7M_D$ .

First it can be extrapolated that even on best cells (lowest achieved  $M_D$  values @ 0.14) the removal of all the defectivity would yield a +1.5% abs. power conversion efficiency. Nonetheless care must be taken performing such an extrapolation to  $M_D = 0$  since one cannot foresee the behaviour of  $\eta = f(M_D)$  for  $M_D \rightarrow 0$ .

Then another way to quantify the performance loss due to the defectivity is to project the efficiency dispersion as seen in Figure 2 to the realistic case (existing handling systems, level reached in practice) where all cells amount the defectivity value  $M_D$  corresponding to the 25% best  $M_D$  values,  $M_{D,25\%}$ . The resulting distribution curves are shown in Figure 3.

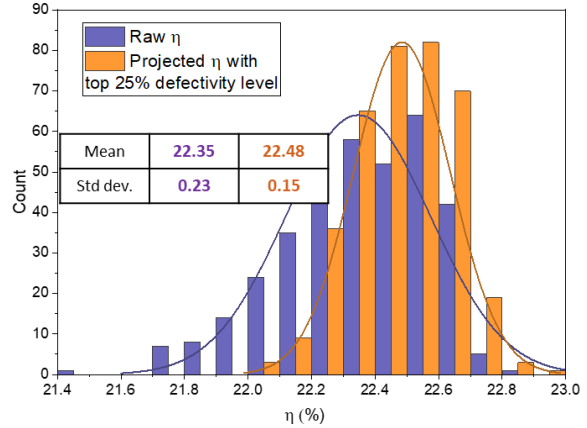


Figure 3: Power conversion efficiency distribution for cells as measured (violet) and projected as if their defectivity amounts the mean 25% best  $M_D$  values of the original distribution (orange).

This projection would lead to a power conversion efficiency increase of +0.13% in this example. Last but not least, the dispersion is reduced by 30%.

### 4 HETLUMTOOL AS A HELP FOR DEVISING AUTOMATION PARTS CLEANING STRATEGY

The ability to detect any changes in the behavior of the production line before their effect on device performance become critical is essential to keep the productivity at high level. This statement is illustrated in Figure 4 where the cell efficiency  $\eta$  is plotted as a function of the global defectivity  $M_D$  for 2 batches of cells produced *before* and *after* cleaning the automatic transport system (automation: belts, vacuum pickers) at Plasma Enhanced Chemical Vapour Deposition (PECVD) stage.

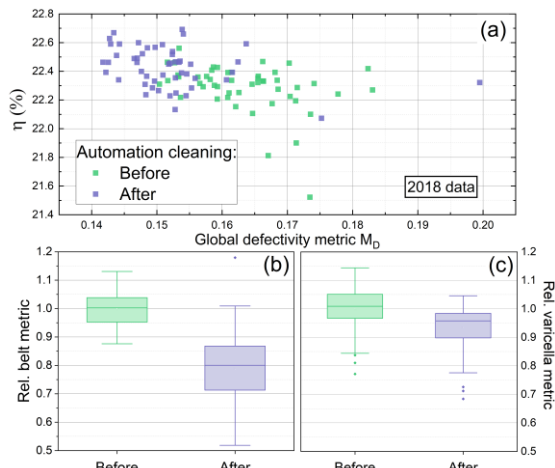


Figure 4: (a) Cell performance versus defectivity metric  $M_D$  before and after automation parts cleaning. (b) Relative belt marks metric before/after cleaning the automation parts. (c) Relative varicella (punctual, random defects) metric before/after cleaning the automation parts

In Figure 4 (a), one observes that automation parts cleaning has a clear beneficial impact, noticeable on cell efficiency gaining about 0.15% absolute. In addition, the defectivity distribution shifted to lower  $M_D$  values, confirming the fact that the efficiency gain attributed to the action on the automation is associated with a lowering of the defectivity. More in details, the global defectivity is decomposed into two components (belts marks and varicella) in Figure 4 (b) and (c). The reduction in the defectivity linked to the contact of the wafers with the conveyor belts is more pronounced than the reduction of the varicella defectivity, the later originating from contact of the wafer over its whole surface with vacuum pickers or trays.

From this example, through the help of HETLUMTOOL, one can conclude that it is more efficient to clean the belts. This application case can even be seen otherwise: instead of running a dedicated experiment, one could track the evolution in time of the belt metric. On a production line, the staff would be warned when the metric starts drifting, meaning that an intervention on the line is required. The image processing time is compatible with current production tact time: all cells can be monitored over a long period of production.

Conveniently, the image processing does not require the cell to be finished to be performed. Right after the passivation of both sides of the wafer, a PL image can be acquired. In practice it is preferable waiting that the passivating nano-layers are protected (with ITO for example in the case of SHJ): in such a way it is more unlikely that further degradation of the passivation occurs on the rest of the production line. Doing so, drift of the defectivity can be identified very early and avoid unnecessary material consumption on low quality cells.

## 5 MINIMAPS: TOWARD CLUSTERING AND BIG DATA ANALISYS

In an industrial context, the amount of data generated via PL and HETLUMTOOL is very large, one

image being typically 1024x1024 pixels. Additionally, the ability to compare two cells with each other, or two groups of cells (going through different lines or equipment for instance) is crucial. However, the pixel-to-pixel comparison is slow and computer-intensive and would generate uncertain results since the cells can be slightly shifted or rotated in the images, and recurring defects themselves might not exactly be always at the same place. On the contrary comparing only the metric goes with a loss of data since all spatial information is lost.

### 5.1 Minimap concept

The proposed solution lies in the middle ground between global metrics and pixel-to-pixel comparisons. The image is first projected onto a purposefully coarse grid, of  $16 \times 16$  pixels for example. For each of the small grid elements, scores are computed, corresponding to the local value of the considered metric. The scores are then reported into small matrices, that are called *minimaps*. The process for obtaining a minimap is depicted in Figure 5.

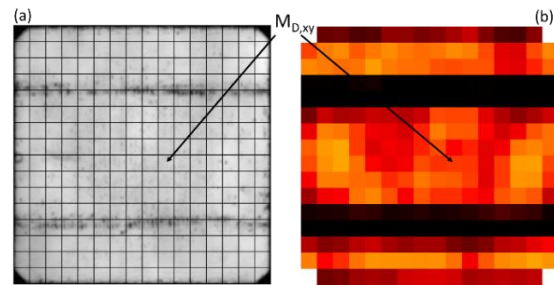


Figure 5: Generation of a minimap from a raw image (a) going through the HETLUMTOOL image processing, then divided into a coarse 16x16 matrix filled with the local defectivity metric  $M_{D,xy}$  value (b).

Minimaps being very small matrices, their manipulation is far less computationally expensive. Two minimaps can be compared using a simple Euclidian distance.

Via minimaps, the comparison between large number of cells is now possible, which opens the way to clustering.

### 5.2 Towards clustering

On cells produced with a given industrial setup, the images are very similar, forming a dense, uniform cloud. Besides the individual outliers, some less dense, off center points may reveal some factory issues that are worth examining. Ward's method [7] was used to perform clustering. For the visualization of the  $16 \times 16 = 256$  dimension vectors that are the minimaps, Principal Component Analysis (PCA) was used. It tries to place orthogonal axes in the point cloud that can best explain its variance: each axis is represented by a vector, and the points are linear combinations of these vectors. Hence the PCA vectors often represent defects in the batch that can be independent.

A typical PCA plot showing the results of the clustering algorithm applied to a batch of cell produced at CEA is represented in

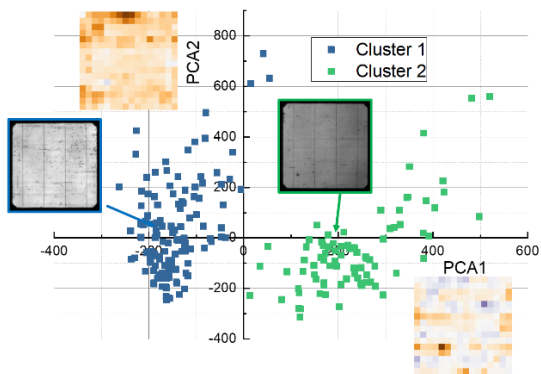


Figure 6.

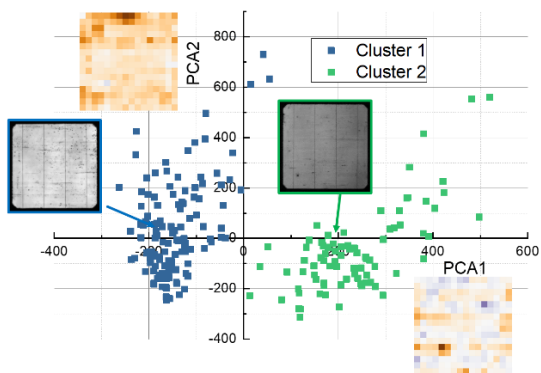


Figure 6: Principal component analysis (PCA) based clustering on cells produced on Labfab (partly intentionally degraded for clarity purposes), together with cell instances from each cluster.

The automatic definition of clusters in this batch of cells identified two clusters. Both clusters are placed at different PCA1 unit values, highlighting the fact that they differentiate from each other because of the defect present in the bottom left quarter of PCA1 unit minimap. Cell instance PL images are shown in

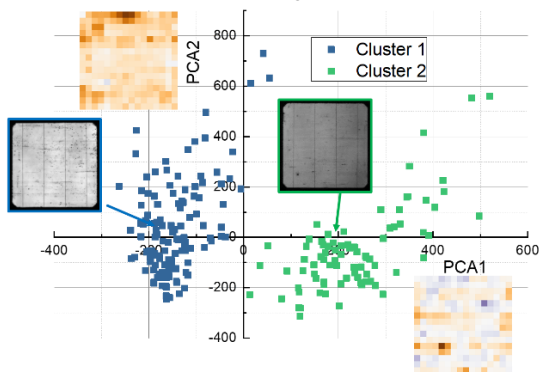


Figure 6 for each cluster: as a matter of fact the remarkable feature between cluster 1 and cluster 2 is the punctual defect.

Other application cases were tested recently and very subtle defects were revealed thanks to the clustering.

## 6 CONCLUSION

An image processing software was developed at CEA to quantify and analyze the defectivity present on SHJ

cells. Several defectivity metrics were defined to precisely characterize how the local lack of passivation affects the cell performance. For use in an industrial context where the amount of data increases considerably with line throughput, the minimap concept (coarse spatial representation of the cell defectivity) was introduced.

The gap between best cells and the ideal case at 0 defectivity is estimated to be 1.5% abs. It was also proven that taking care of the handling systems is necessary to keep the production line at its highest level, with a low dispersion.

The method introduced here is applicable not only to SHJ cells, but to a wide variety of cell technologies including PERC, TopCon, back contact cells, etc.

Working on reducing defectivity has taken an important part in the cell performance increase at CEA over the last 2 years. As a consequence, a champion cell at 24.63% was certified on total area (244.3 cm<sup>2</sup>), and more recently CEA achieved 25.00% (212.84 cm<sup>2</sup>).

## BIBLIOGRAPHY

- [1] X. Ru *et al.*, “25.11% efficiency silicon heterojunction solar cell with low deposition rate intrinsic amorphous silicon buffer layers,” *Solar Energy Materials and Solar Cells*, vol. 215, p. 110643, Sep. 2020, doi: 10.1016/j.solmat.2020.110643.
- [2] “CEA Press release - SHJ 24.63%.” <http://liten.cea.fr/cea-tech/liten/english/Pages/Medias/News/PV-High-Efficiency/New-heterojunction-solar-cell-efficiency-record-certified.aspx> (accessed Aug. 24, 2020).
- [3] O. Nos *et al.*, “Quality control method based on photoluminescence imaging for the performance prediction of c-Si/a-Si:H heterojunction solar cells in industrial production lines,” *Solar Energy Materials and Solar Cells*, vol. 144, pp. 210–220, Jan. 2016, doi: 10.1016/j.solmat.2015.09.009.
- [4] Valentin Giglia, J. Veirman, Renaud Varache, and Erwann Fourmond, “Understanding of the Influence of the Surface Defectivity on Silicon Heterojunction Cell Performance,” *36th European Photovoltaic Solar Energy Conference and Exhibition*, Marseille, France, pp. 358–363, 2019.
- [5] Valentin Giglia, Renaud Varache, Jordi Veirman, and Erwann Fourmond, “Understanding the influence of localized surface defectivity properties on the performances of SHJ cells,” *PROGRESS IN PHOTOVOLTAICS*, 2020.
- [6] B. Hallam, B. Tjahjono, T. Trupke, and S. Wenham, “Photoluminescence imaging for determining the spatially resolved implied open circuit voltage of silicon solar cells,” *Journal of Applied Physics*, vol. 115, no. 4, p. 044901, Jan. 2014, doi: 10.1063/1.4862957.
- [7] Joe H. Ward Jr., “Hierarchical Grouping to Optimize an Objective Function,” *Journal of the American Statistical Association*, vol. 58, no. 301, pp. 236–244, 1963.